

# Distributed Planar Manipulation in Fluidic Environments

Guillaume Sartoretti<sup>1</sup>, Samuel Shaw<sup>2</sup> and M. Ani Hsieh<sup>3</sup>

**Abstract**—We present a distributed control strategy that enables a swarm of autonomous surface vehicles (ASVs) to cooperatively grasp and manipulate a large floating object from an initial position and orientation to a desired final position and orientation. Given an initial set of random robot positions, our control strategy enables the team to synchronize their arrival times around the object. Analytical motion trajectories are then computed to enable the swarm to transport the object to the final desired position. We validate the proposed strategy in simulation and present experimental results to demonstrate the feasibility of the proposed strategy.

## I. INTRODUCTION

As robotic swarm sizes can vary over time, we are interested in developing scalable control strategies that can adapt to changing team sizes and that are resistant to single robot failures. These properties can often be achieved via a distributed control framework with the added benefit of robustness due to the inherent redundancy resulting from having a large number of similar robots. In this paper, we consider the problem of collective transport of an object in a fluidic environment by a team of autonomous robots. We build upon [1] to devise a distributed Braitenberg-inspired control mechanism, allowing the autonomous surface vehicles (ASVs) to move along smooth trajectories as they approach, grasp and manipulate a larger object in a fluid environment.

Previous works on cooperative manipulation of large objects by teams of ground robots include [2]. In this work, the collective transport of convex and non-convex objects is achieved by enabling the team to first surround and cage the object of interest and then transport through the synthesis and composition of appropriate artificial potential functions. More recently, a decentralized control strategy for manipulation of a general-shaped object by a swarm of ground vehicles equipped with grippers was presented in [3]. However, these strategies do not directly translate to the fluid environment due to the unique challenges associated with the near frictionless environment, *e.g.*, objects floating on the surface, and non-negligible inertial effects. Existing work in autonomous collective transport in marine and

littoral environments include [4]. In [4], the authors devised a decentralized control strategy for a swarm of tugboats to cooperatively rotate a larger object. Similar work on cooperative manipulation by a team of tugboats to transport a larger vessel is described in [5], [6].

Different from [4], [5], [6], our main contribution is the construction of a set of acceptable trajectories, allowing a swarm of ASVs to transport an object from any given initial pose to any desired final pose under Conditional Closure (CC). Rather than rely on towing cables, collective manipulation and transport is achieved by enabling the swarm to “grasp” the larger object and achieve CC through coordinated pushes. Specifically, we leverage the structure-fluid interaction between the transported object and the fluid environment in our formulation of “conditional forced caging” and leverage the vehicle’s and object’s inertial effects to achieve synchronized arrival times to achieve CC of the object. We validate our strategy in simulation and show the feasibility and validity of the strategy through experiments.

The paper is organized as follows: in Section II, we briefly presents the considered problem. In Section III, we define the two main phases of our control mechanism, and present numerical results. Section IV is devoted to our experimental results, while Section V discusses of the future perspectives.

## II. PROBLEM STATEMENT

We consider a swarm of  $N$  autonomous ASVs operating in a still body of water. We model the  $i^{th}$  ASV as a two-dimensional (2D) differential vehicle whose kinematics in discrete time are given by

$$\begin{cases} V_{L,i}(t+1) &= S_{*,i} + \beta \cdot \cos[h_i(t) - \alpha_i(t) \\ &\quad + (\frac{\pi}{2} - \phi_i(t))], \\ V_{R,i}(t+1) &= S_{*,i} - \beta \cdot \cos[h_i(t) - \alpha_i(t) \\ &\quad + (\frac{\pi}{2} - \phi_i(t))], \end{cases} \quad (1)$$

where  $V_{L,i}$  and  $V_{R,i}$  denotes the left and right propeller speeds,  $(x_i, y_i)$  the current position,  $S_{1,i}$  the speed, and  $\alpha_i$  the angle of the vector  $[x_i - Tx, y_i - Ty]^T$  in the global coordinate frame. In this work, we assume  $S_{*,i}$  to be constant. We note that the vehicle kinematics given by (1) define a general Braitenberg control mechanism [7] allowing an ASV to move at a constant speed, keeping a given point  $T = [Tx, Ty]^T$  at a given angle  $\phi$  from its heading. The angle  $\phi$  defines the desired difference between the angular position of a robot, and its heading  $h$ . For example, when  $\phi = \frac{\pi}{2}$ , the ASV simply revolves around the point  $T$  (*i.e.*,  $T$  is the instantaneous center of rotation for the ASV, remaining at an angle of  $\frac{\pi}{2}$  from the ASV’s heading). Fig. 1 illustrates

We gratefully acknowledge the support of ONR Award Nos. N000141211019 and N000141310731 and National Science Foundation (NSF) grant IIS-1253917. Guillaume Sartoretti is funded by the Swiss National Science Foundation.

<sup>1</sup>Guillaume Sartoretti is with the Laboratory of Microengineering for Manufacturing, Ecole Polytechnique Fédérale de Lausanne, 1015 Lausanne, Switzerland [guillaume.sartoretti@epfl.ch](mailto:guillaume.sartoretti@epfl.ch)

<sup>2</sup>Samuel Shaw is with The Haverford School, PA 19041, USA [samushaw@haverford.org](mailto:samushaw@haverford.org)

<sup>3</sup>M. Ani Hsieh is with the Scalable Autonomous Systems Laboratory, Mechanical Engineering, Drexel University, Philadelphia, PA 19104, USA [mhsieh1@drexel.edu](mailto:mhsieh1@drexel.edu)

the situation at a given time and depicts the various relevant quantities.

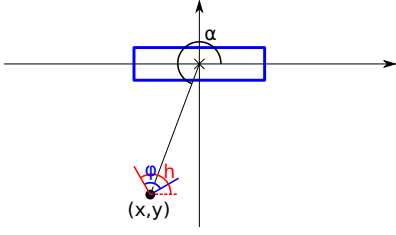


Fig. 1. (a) Schematic of the relevant quantities for the Braitenberg control mechanism given by (1). Here,  $T = \mathbf{O} = (0,0)$  with the object (blue rectangle) and an ASV (black dot) located at position  $(x,y)$ . The ASV's heading  $h$  is illustrated in red and its angular position  $\alpha$  in black. A desired angle  $\phi$ , defining the desired difference between  $\alpha$  and  $h$ , is shown in blue.

Given a large object, which we will represent as a rectangle in 2D, that is initially centered at the origin,  $\mathbf{O} = (0,0)$ , of the global frame, we assume that the object is positioned such that its length lies along the global  $X$ -axis. The objective is to devise a collective transport strategy such that the swarm encloses or “grasps” the object and transports it to a final pose  $[x_f, y_f, h_f]^T$  where  $h_f$  denotes the orientation of the object. To achieve this, we decompose the problem into two separate phases: the “grasping” and transport phases. We describe our methodology in the following section.

### III. PLANAR MANIPULATIONS UNDER CONDITIONAL FORCED CAGING

#### A. Distributed Approach and Grasp

We assume vehicles are initially randomly positioned within the workspace. “Grasping” is achieved by aligning the vehicles on one side of the object, facing the object (namely, on the side where  $y > 0$ ). This will enable the team to transport the object by cooperatively pushing the object towards its pose. To achieve this, we assign each robot a target point  $T_i$  ( $1 \leq i \leq N$ ) to aim for as it approaches the object. We choose  $T_2, \dots, T_{N-1}$  such that they are uniformly distributed along the central axis of the object, while  $T_1$  and  $T_N$  are placed at each end of the object. This allows the swarm to hold the object under Conditional Closure (CC) once the object is “grasped” (see Fig.2a) [8].

To achieve this, we set  $S_{*,i} = S_{1,i}$  in (1) where  $S_{1,i}$  is the constant approach speed and  $\alpha = \arctan\left(\frac{y_i - T_{y_i}}{x_i - T_{x_i}}\right)$ . The kinematics given by (1) allows a robot to rotate around the origin point in a clockwise direction for  $\phi = \frac{\pi}{2}$ , and in a counter-clockwise direction for  $\phi = 3\frac{\pi}{2}$ . For robots starting in the half-plane  $\{x > 0\}$ , we want them to rotate in the counter-clockwise direction to reach their destination faster. To achieve this, we let  $D \in \{0, 1\}$  denote each robot's direction of rotation (clockwise (0) or counter-clockwise (1)). An ASV starting in the half-plane  $\{x < T_i\}$  is assigned  $D = 0$ , and an ASV starting at initial position  $x_{0,i} \geq T_i$  receives  $D = 1$ . A correction is then made to (1) to encompass this rotation direction, by changing  $\phi_i(t) \rightarrow \phi_i(t) + D\pi$ .

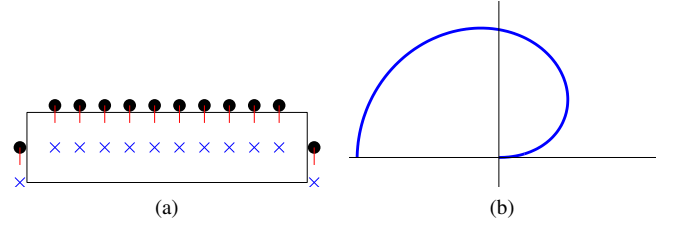


Fig. 2. (a) Example of conditional closure (CC), where the pushing ASVs (black dots) are able to translate and rotate the object, with constraints on the translation direction and the rotation pivot. The target points are depicted as blue crosses, and the ASVs' heading vectors as red segments). (b) Typical shape of the spiral of Eq.(4), with  $r_\pi = 1$ . Here,  $\theta = \arcsin(\alpha, \frac{\pi}{2})$ , meaning that both axes are simply switched.

To obtain a spiral-shaped motion from the initial position of the robot until its perpendicular approach to the object's side, we now let  $\phi$  depend on the angular position of each robot. We want  $\phi \approx \frac{\pi}{2}$  when the robot is in the lower half-plane  $\{y < 0\}$  (i.e., pure rotation around the origin point). We then want  $\phi$  to gradually decrease toward  $\phi = 0$ , as  $\alpha$  approaches  $\frac{\pi}{2}$  (i.e., pure attraction to the origin point). We let  $\phi$  exponentially decrease, as  $\alpha$  approaches  $\frac{\pi}{2}$ :

$$\phi_\sigma(\alpha) = \frac{\pi}{2} \left( 1 - \exp\left(-\frac{\arcsin(\alpha, \frac{\pi}{2})}{\sigma}\right) \right), \quad (2)$$

where  $\sigma^2 \in \mathbb{R}^+$  controls the rate of exponential decay. We write  $\arcsin(\theta_1, \theta_2)$  as the minimal angle difference between  $\theta_1$  and  $\theta_2$ :

$$\arcsin(\theta_1, \theta_2) := \min \left( \begin{array}{l} \text{mod}(\theta_1 - \theta_2, 2\pi) \\ \text{mod}(\theta_2 - \theta_1, 2\pi) \end{array} \right).$$

We finally incorporate  $\phi_\sigma(\alpha)$  into Eq.(1) to obtain the final control mechanism for our robotic swarm. Note how  $\phi_\sigma(\alpha)$  must also be corrected with regard to  $D$ , to obtain suitable dynamics for both turning directions:

$$\begin{cases} V_{L,i}(t+1) &= S_{1,i} + \beta \cdot \cos [h_i(t) - \alpha_i(t) + \frac{\pi}{2} \\ &\quad + D\pi - (2D-1)\phi_\sigma(\alpha_i(t))], \\ V_{R,i}(t+1) &= S_{1,i} - \beta \cdot \cos [h_i(t) - \alpha_i(t) + \frac{\pi}{2} \\ &\quad + D\pi - (2D-1)\phi_\sigma(\alpha_i(t))], \end{cases} \quad (3)$$

1) *Computation of the Approaching Speeds:* Given (3), a robot starting at any given initial position moves along a spiral-shaped trajectory toward its given target point  $T$ . We now want all robots to converge to their targets  $T_i$  at a desired given time  $T_{goal}$ . The correct synchronization of the arrival times allows the robots to start pushing the object all at once. To do this, we estimate the length of the resulting individual robot trajectories resulting from the Braitenberg control mechanism given by (3) as exponential spirals. We express a spiral as a function of the radius of each point of the spiral with respect to its angular position. To simplify the expression, we rotate the frame of reference, and measure the angular position  $\theta$  of the spiral's points starting from the angle  $\frac{\pi}{2}$ . In our case, our spirals are defined for any angular position  $\theta \in [0, \pi]$ , where, because of symmetries, robots

cannot move more than half a circle around their target point. Using the relation for  $\phi_\sigma(\alpha)$ , our approximate spiral is:

$$r(\theta) := r_\pi \left( 1 - \exp\left(-\frac{\theta}{\sigma}\right) \right). \quad (4)$$

The typical shape of the spiral, with  $r_\pi = 1$ , is shown in Fig. 2b. In our case, we need to let each robot compute  $r_\pi$ , from its initial position  $(r_0, \theta_0)$ , where  $\theta_0 = \arccos(\alpha_0, \frac{\pi}{2})$ . This is achieved by putting  $r_0$  and  $\theta_0$  in (4), and by extracting  $r_\pi$  we get  $r_\pi = r_0 / (1 - \exp(-\frac{\theta_0}{\sigma}))$ . With the expression of the spiral for the trajectories' shapes, we can now obtain the trajectories lengths from the initial position of each robot. The initial angular and radial positions of each robot are first computed with respect to their target point:

$$\begin{cases} r_0 = \sqrt{(x_0 - T_x)^2 + (y_0 - T_y)^2} \\ \theta_0 = \arccos(\arctan \frac{y_0 - T_y}{x_0 - T_x}, \frac{\pi}{2}). \end{cases}$$

We then compute the length of the spiral following Eq.(4), from the initial position to the target point, as:

$$L_i(r_0, \theta_0) = \int_0^{\theta_0} \sqrt{r(\theta)^2 + \left(\frac{d}{d\theta}r(\theta)\right)^2} d\theta,$$

which yields a lengthy but exact result, given in Eq.(5).

With this analytical expression for the trajectory length of an ASV starting at any initial position, we are able to adapt the individual speeds  $S_{1,i}$  of each ASV. We let the approach speed of each ASV depend on its trajectory length  $L_i(r_0, \theta_0)$  in order to let the ASVs meet their target point in the vicinity of a desired time  $T_{goal}$ :

$$S_{1,i} = S_{1,i}(r_0, \theta_0) = \frac{L_i(r_0, \theta_0)}{T_{goal}}. \quad (6)$$

2) *Link with Brownian Swarms:* Eq.(3) can be translated into a set of differential equations to model the multi-agent swarm dynamics. We identify the ASVs as Brownian agents in  $\mathbb{R}^2$  with the following dynamics expressed in polar coordinates:

$$\begin{cases} dr_i(t) = -S_{1,i} \cdot \exp\left(-\frac{\arccos(\alpha_i(t), \frac{\pi}{2})}{\sigma}\right), \\ d\alpha_i(t) = (2D - 1) \frac{S_{1,i}}{r_i(t)} \left(1 - \exp\left(-\frac{\arccos(\alpha_i(t), \frac{\pi}{2})}{\sigma}\right)\right). \end{cases} \quad (7)$$

Noise can be added to (7) in the form of White Gaussian noise to model any actuators and/or sensors uncertainty. This effectively allows us to express the global swarm dynamics as a set of  $N$  stochastic differential equations (SDE). Conventional tools of dynamical systems theory can be used on the resulting nonlinear SDEs to study the probability distribution of the swarm's position during the approach. Note that, similar to the original Braitenberg control, the norm of the instantaneous speed of each agent remains constant through time  $v_i(t) = r(t)d\alpha(t)/dt + dr(t)/dt = S_{1,i} \forall t$ .

### B. Computation of the Manipulation Trajectories

It is important to note that in the absence of an external flow field, by aligning the vehicles along one side of the object as shown in Fig. 2a is sufficient to achieve CC. Furthermore, in this configuration, the robots can only

translate the object towards the half-plane  $\{y \geq 0\}$  and any rotation applied to the object under CC cannot have its pivot point within the object. Therefore, the distance between the barycentric position of the object, and the pivot point must be at least  $\frac{S_x}{2}$ , *i.e.*, half the object's length. These constraints define a set of allowed translations and rotations, which the swarm can apply to the object under CC. As such, the objective in the second phase is to synthesize a strategy enabling the swarm to maintain CC while transporting the object to the desired final pose  $[x_f, y_f, h_f]^T$  given its initial pose of  $x_0 = y_0 = h_0 = 0$ .

In this second phase, the ASVs will be modeled and controlled via (3), however their forward speeds,  $S_{*,i}$ , will be adapted to translate/rotate the object. To achieve this, we restrict the object's motion to circular arcs only. In fact, given an initial pose of the object, it is possible to move the object to any desired pose by moving the object along a trajectory composed of two well chosen circular arcs. To show this, we let the object first travel along an arc of length  $\alpha_1$  around the center  $[C_{1,x}, C_{1,y}]^T$  of a first circle  $C_1$  followed by a motion along an arc of length  $\alpha_2$  around the center  $[C_{2,x}, C_{2,y}]^T$  of a second circle  $C_2$ . We first note that  $C_{1,y} = 0$ , since the vector  $[C_{1,x} - x_0, C_{1,y} - y_0]^T$  must be perpendicular to the object's initial orientation, *i.e.*, the vector initially given by  $[1, 0]^T$ . This ensures that the  $[C_{1,x} - x_0, C_{1,y} - y_0]^T$  is tangent to  $C_1$ , since the object's heading faces the center of  $C_1$ . The constraints of our system can then be expressed as follows:

- 1) We know that after the first arc  $\alpha_1$ , the orientation of the object is  $\alpha_1$ . After the second arc, the final orientation must therefore verify:

$$h_f = \alpha_1 + \alpha_2. \quad (8)$$

- 2) Using the 2D rotation matrix  $M_\alpha$ , we can compute the successive positions of the object after traveling along each of the two arcs. After the first arc, the object ends up at the position  $(x_1, y_1)$ , with

$$\begin{aligned} \begin{pmatrix} x_1 \\ y_1 \end{pmatrix} &:= M_{\alpha_1} \cdot \begin{pmatrix} x_0 - C_{1,x} \\ y_0 - C_{1,y} \end{pmatrix} + \begin{pmatrix} C_{1,x} \\ C_{1,y} \end{pmatrix} \\ &= \begin{pmatrix} C_{1,x} \cdot (1 - \cos(\alpha_1)) \\ -C_{1,x} \cdot \sin(\alpha_1) \end{pmatrix}. \end{aligned} \quad (9)$$

From this intermediate position, the object then follows an arc length  $\alpha_2$  around the center of  $C_2$ . The final position must equal  $(x_f, y_f)$ , which gives us a second relation:

$$M_{\alpha_2} \cdot \begin{pmatrix} x_1 - C_{2,x} \\ y_1 - C_{2,y} \end{pmatrix} + \begin{pmatrix} C_{2,x} \\ C_{2,y} \end{pmatrix} = \begin{pmatrix} x_f \\ y_f \end{pmatrix}. \quad (10)$$

- 3) Finally, the vector  $[x_1 - C_{2,x}, y_1 - C_{2,y}]^T$  must be perpendicular to the object's normal vector after the first arc. This condition, similar to  $C_{1,y} = 0$ , ensures that at  $(x_1, y_1)$ , the object is simultaneously on both circles  $C_1$  and  $C_2$ .

$$\begin{aligned} \begin{pmatrix} x_1 - C_{2,x} \\ y_1 - C_{2,y} \end{pmatrix} \cdot M_{\alpha_1} \cdot \begin{pmatrix} 1 \\ 0 \end{pmatrix} &= \\ (C_{2,x} - C_{1,x}) \cdot \sin(\alpha_1) - C_{2,y} \cdot \cos(\alpha_1) &= 0. \end{aligned} \quad (11)$$

$$L_i(r_0, \theta_0) = r_0 \left( \frac{1}{e^{\theta_0/\sigma} - 1} + 1 \right) \left[ \left( 1 - \frac{\sigma^2 \log(\sqrt{\sigma^2+1}+1)}{\sqrt{\sigma^2+1}} \right) - e^{-\frac{\theta_0}{\sigma}} \sqrt{\sigma^2 (e^{\theta_0/\sigma} - 1)^2 + 1} + \frac{\sigma^2 \log \left( e^{-\frac{\theta_0}{\sigma}} \left( \sigma^2 (1 - e^{\theta_0/\sigma}) + \sqrt{\sigma^2+1} \sqrt{\sigma^2 (e^{\theta_0/\sigma} - 1)^2 + 1} + 1 \right) \right)}{\sqrt{\sigma^2+1}} - \sigma \sinh^{-1}(\sigma - \sigma e^{\theta_0/\sigma}) \right]. \quad (5)$$

With these 4 equations, and 5 variables  $\{\alpha_1, \alpha_2, C_{1,x}, C_{2,x}, C_{2,y}\}$ , we are left with one degree of freedom. We choose to fix  $\alpha_1$ , and to compute the values of the other variables accordingly. After solving Eqs(8)-(11), with  $\alpha_1$  fixed, we end up with:

$$\begin{cases} \alpha_2 &= h_f - \alpha_1 \\ C_{1,x} &= -\frac{1}{2} \csc\left(\frac{\alpha_1}{2}\right) \csc\left(\frac{\alpha_1+\alpha_2}{2}\right) \left(x_f \cos\left(\alpha_1 + \frac{\alpha_2}{2}\right) + y_f \sin\left(\alpha_1 + \frac{\alpha_2}{2}\right)\right) \\ C_{2,x} &= \frac{1}{2} \csc\left(\frac{\alpha_2}{2}\right) \csc\left(\frac{\alpha_1+\alpha_2}{2}\right) \left(x_f \cos\left(\frac{\alpha_1}{2}\right) + \sin\left(\frac{\alpha_1}{2}\right) (y_f \cos(\alpha_1 + \alpha_2) - x_f \sin(\alpha_1 + \alpha_2))\right) \\ C_{2,y} &= \cos\left(\frac{\alpha_1}{2}\right) \csc\left(\frac{\alpha_2}{2}\right) \left(x_f \cos\left(\frac{\alpha_1+\alpha_2}{2}\right) + y_f \sin\left(\frac{\alpha_1+\alpha_2}{2}\right)\right) \end{cases} \quad (12)$$

To avoid sharp corners in the resulting object trajectory, we must check for situations when the resulting trajectory exhibits a kink and correct  $\alpha_1$  accordingly:

$$\tilde{\alpha}_1 := \begin{cases} \alpha_1 - 2\pi & \text{if } \text{sign}(\alpha_1) = \text{sign}(C_{1,x}), \\ \alpha_1 & \text{otherwise.} \end{cases} \quad (13)$$

An example is shown in Fig. 3 where an initial motion in the  $y > 0$  direction results in a kinked trajectory. Note that this does not change the final position  $(x_1, y_1)$  of the object after the first arc. Similarly, To ensure the trajectory is continuous at  $(x_1, y_1)$ , must also set  $\alpha_2$  accordingly. By resetting the reference frame of reference at the position  $(x_1, y_1)$  to the orientation  $\alpha_1$ :

$$\begin{pmatrix} \tilde{C}_{2,x} \\ \tilde{C}_{2,y} \end{pmatrix} = M_{-\alpha_1} \cdot \begin{pmatrix} C_{2,x} - x_1 \\ C_{2,y} - y_1 \end{pmatrix}$$

we can check that  $\alpha_2$  and  $\tilde{C}_{2,x}$  have the same sign and set  $\alpha_2$  accordingly:

$$\tilde{\alpha}_2 := \begin{cases} \alpha_2 - 2\pi & \text{if } \text{sign}(\alpha_2) = \text{sign}(\tilde{C}_{2,x}), \\ \alpha_2 & \text{otherwise.} \end{cases} \quad (14)$$

Fig. 3 shows an incorrect trajectory corrected using this method, enabling us to obtain a smooth trajectory following only allowed translations/rotations under CC.

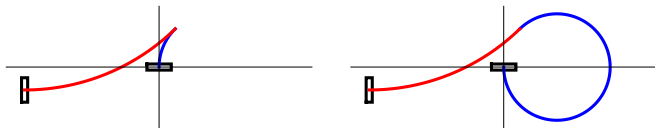


Fig. 3. Example trajectory where  $\alpha_1$  must be corrected (left), and the corrected trajectory using Eq.(14) (right). The initial and final states of the object are shown in black.

1) *Computation of the Pushing Speeds:* Once we find the centers of the circles  $C_1$  and  $C_2$  for an acceptable trajectory, we let the speed of each robot in the swarm depend on its distance to the center of the circle the object is traveling on. Let  $P(t) = \{P_x(t), P_y(t)\}$  be the instantaneous position of the barycenter of the caged object at time  $t$ , we let the speed of the robot  $i$  at time  $t$  be  $V_i(t) = \bar{S}_2 \|X_i(t) - C\| / \|P(t) - C\|$  where  $C$  denotes the center of the circle the object is currently traveling on, and  $\bar{S}_2$  is the desired average speed of the object along the trajectory. Robots switch from  $C = C_1$  to  $C = C_2$  when  $P(t) \approx (x_1, y_1)$  as given by (9).

*Remark 1:* We note that the computed object transport trajectories are similar to Dubins paths for general non-holonomic vehicles with unicycle dynamics [9], [10]. Rather than trajectories composed of circular arcs of the same radii, our paths are composed of trajectories composed of two arcs of different radii. Additionally, the circular arc segments in optimal Dubins paths are dictated by the vehicle's smallest turning radius. In fluidic environments, it may be difficult to manipulate the object to achieve such a tight turning radius since this would require one of the end ASVs, *i.e.*, one of the ASVs caging the plank along its main axis, to serve as the rotational pivot. While this maneuver may be manageable for ground vehicles, it is generally much harder for surface marine vehicles. As such, we opt for computing our suboptimal trajectories rather than employ their optimal Dubins counterpart.

## IV. RESULTS

### A. Simulation Results

To validate our collective transport strategy, we present two simulation scenarios with  $N = 4$  and  $N = 8$  robots as shown in Fig. 4 and 5. In the simulation, we assume that the sum of the ASVs' weights is equal to the individual weight of the object being transported. This helps to synchronize the transport phase by preventing early arriving ASVs from being able to rotate the object too fast on their own. The push phase starts when the whole swarm has arrived at their assigned target points around the object. The approach speeds of the ASVs are computed to synchronize their arrival around  $T_{goal} = 30 s$ . The arc length around the first circle is selected to be  $\alpha_1 = 1$ , and the trajectory is computed in order to position the object at  $\{x_f, y_f, h_f\} = \{55, -95, 0.1\}$ .

In our simulations, white Gaussian noise was added to each robot's pose at each timestep with a variance of 0.05 for each component. The vehicle speeds are computed using (3) were updated at 50 Hz. Fig. 4b shows the synchronized arrival of the ASVs around the object. Fig. 5 shows the complete trajectories of a swarm of  $N = 8$  ASVs transporting an object for two different initial and final poses.

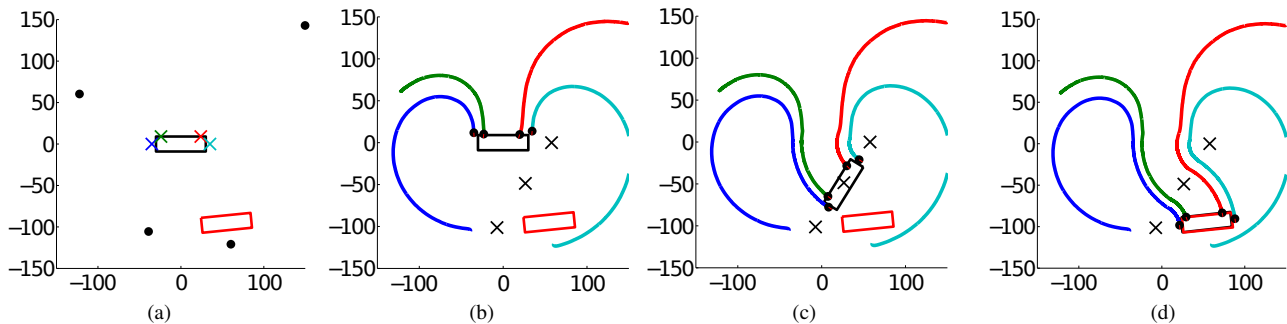


Fig. 4. A swarm of  $N = 4$  ASVs (black dots) push the large object (black rectangle) towards the final position  $\{x_f, y_f, h_f\} = \{55, -95, 0.1\}$  (red rectangle) at different times during the simulation.

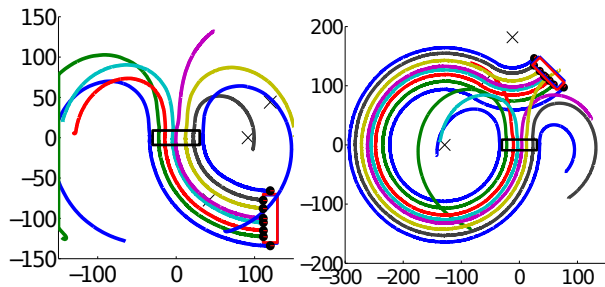


Fig. 5. Complete trajectories of a swarm of  $N = 8$  ASVs (black dots), moving a object to its final position (red rectangle). The object is initially positioned at  $\{x_0, y_0, h_0\} = \{0, 0, 0\}$ . The two circles' centers, and the intermediate switching point, are depicted as black crosses.

## B. Experimental Setup

To experimentally validate our proposed strategy, we employ the multirobot Coherent Structure Testbed (mCoSTe). The mCoSTe is an indoor laboratory experimental testbed that consists of a  $3m \times 3m \times 1m$  flow tank and a fleet of micro-autonomous surface vehicles (mASVs). The mASVs are differential drive surface vehicles, approximately 12 cm long, equipped with a micro-controller board, XBee radio module, and an inertial measurement unit (IMU). Localization for the mASVs and the object being manipulated is provided by an external motion capture system.

The proposed collective transport strategy was validated using a team of  $N = 4$  mASVs. The object being transported is a  $40\text{ cm} \times 15\text{ cm}$  rectangular foam plank with fins attached to the short ends to limit its movement along its main axis. Since the mASV propellers' rotation speeds cannot be linearly translated into a forward speed (as opposed to wheeled mobile robots), Eq.(2) is used to control the vehicles' headings during the approach phase. During the approach and grasping phase, the optimal approach speed for each boat is updated at each iteration ( $dt = 0.1\text{ s}$ ), to synchronize the arrival of all the boats. The targets are re-assigned at each iteration to minimize the likelihood of collision between the vehicles. Target positions around the object are assigned to the nearest mASVs to minimize path crossings between the vehicles. The transport phase only starts when all the vehicles achieve CC around the plank.

Once CC is achieved, the desired final state of the object  $[x_f, y_f, h_f]^T$  is computed in the current body fixed frame of the object and the resulting transport trajectory is computed to move the object to the desired position under CC. In the transport phase, two of the pushing mASVs control the object's orientation along the computed trajectory to ensure the object faces the current circle center while the end vehicles cage the plank along its  $x$  axis and correct the object's motion if it deviates from its main axis. To account for the vehicles' and object's inertia, the vehicles stop prior to arriving at the goal position to ensure the object comes to a stop within range of the final desired pose. Since the object is held under CC, a stopping maneuver cannot be made by the vehicles to ensure the plank is stopped precisely on target. This is a consideration for future work.

## C. Experimental Results

Fig. 6 presents snapshots of the vehicles' trajectories for an experimental run with  $N = 4$  ASVs. During this experimental run, the following values were used:

$$\begin{cases} \sigma = 1 & T_{goal} = 80\text{ s} \\ \alpha_1 = 1 & \{x_f, y_f, h_f\} = \{55, -95, 0.1\}. \end{cases}$$

The initial position of the mASVs (black dots) and the object (black rectangle) is shown in Fig. 6a, along with the targets along the object's side (colored crosses). Fig. 6b shows the vehicles arriving at their assigned target positions, stopping to synchronize and begin the transport phase. The final position and orientation of the object and its transport trajectory was computed from its current pose (red rectangle). The mASVs then started transporting the object while maintaining CC along the computed trajectory (Fig. 6c). Once the final object position was within range ( $20\text{ cm}$ ), the vehicles motors were turned off, letting the object drift to its final position (Fig. 6d).

Fig. 7a-7c present still frames of the experimental results shown in Fig. 6. We ran a series of experimental runs to test the repeatability of the considered control mechanism. The minimal distance from the object's center to the desired final position  $(x_f, y_f)$  was computed for each run, along with the angle error. The measured errors are illustrated in Fig. 7d, along with their respective mean over the 12 experiments. The mean distance error and its standard deviation was

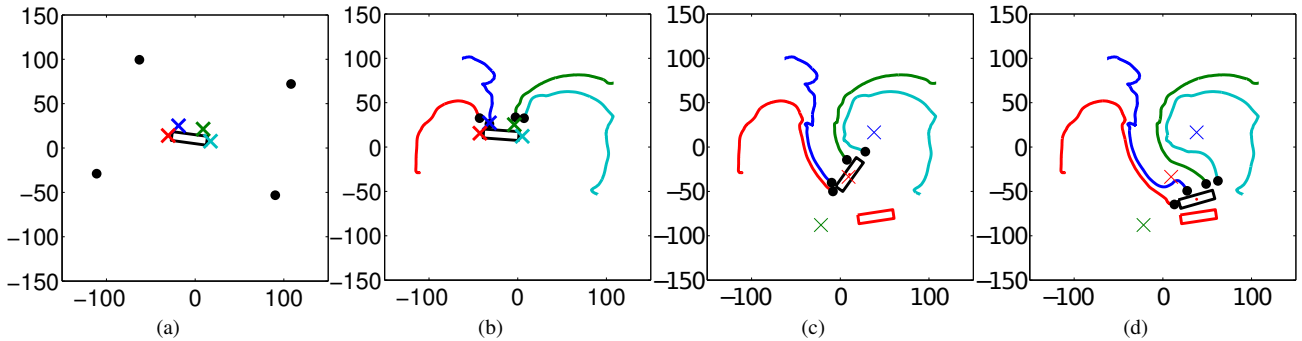


Fig. 6. Snapshots of an experimental run with  $N = 4$  boats. The trajectories (colored lines) of the boats (black dots), are depicted, along with the plank's current position (black rectangle) and its final desired state (red rectangle). During the approach phase, the boats' targets along the plank's side are plotted as colored crosses. During the push phases, the circle centers and intermediate switching points are illustrated as black crosses.

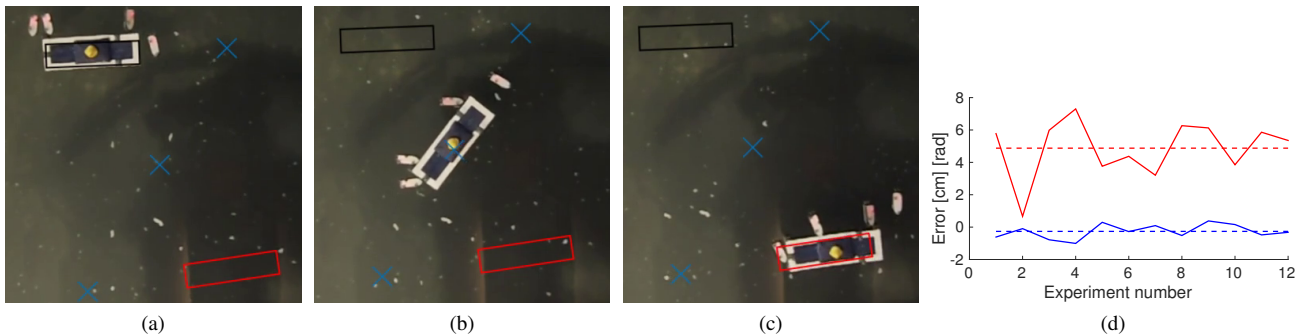


Fig. 7. (a)-(c) Snapshots of an experimental run with  $N = 4$  boats. Initial position of the object is highlighted by the black rectangle and the final desired pose is highlighted by the red rectangle. The circle centers and intermediate switch points are shown by the blue crosses. (d) Position errors (red) and corresponding orientation errors (blue) for the 12 experimental trials. The respective mean errors are shown as dotted lines.

$4.88 \text{ cm} \pm 1.8 \text{ cm}$ , while the mean orientation error and its standard deviation was  $-0.26 \text{ rad} \pm 0.44 \text{ rad}$ .

## V. CONCLUSIONS AND PERSPECTIVES

We have presented a collective transport strategy for a robot swarms manipulating objects in a fluid environment. The strategy enables a team of non-holonomic ASVs to distributively arrange and grasp an object under CC. Despite the fact that this grasping method reduces the set of acceptable translations and rotations of the object, the team can successfully transport it to any position and orientation within the 2D workspace. Simulations and experimental results show the validity of the proposed strategy. Despite the object transport trajectories being sub-optimal, when compared to the corresponding Dubins path, our results suggests the sub-optimal trajectories enable more stable transport by the swarm. Future directions include development of object manipulation strategies for vehicles subject to minimum time, grasp stability, and energy consumption constraints. Lastly, cooperative transport and manipulation by ASV/AUV swarms in a flow field is another direction for future work.

## REFERENCES

- [1] G. Sartoretti, M.-O. Hongler, M. Elias de Oliveira, and F. Mondada, "Decentralized self-selection of swarm trajectories: From dynamical system theory to robotic implementation," *Swarm Intelligence*, vol. 8, no. 4, pp. 329–351, 2014.
- [2] J. Fink, M. Hsieh, and V. Kumar, "Multi-robot manipulation via caging in environments with obstacles," in *IEEE International Conference on Robotics and Automation (ICRA 2008)*, May 2008, pp. 1471–1476.
- [3] G. Habibi, Z. Kingston, W. Xie, M. Jellins, and J. McLurkin, "Distributed centroid estimation and motion controllers for collective transport by multi-robot systems," in *Robotics and Automation (ICRA), 2015 IEEE International Conference on*, 2015, pp. 1282–1288.
- [4] M. Feemster, J. Esposito, and J. Nicholson, "Manipulation of large object by swarms of autonomous marine vehicles, part i: Rotational motions," in *System Theory, 2006. SSTS '06. Proceeding of the Thirty-Eighth Southeastern Symposium on*, March 2006, pp. 205–209.
- [5] J. Esposito, "Distributed grasp synthesis for swarm manipulation with applications to autonomous tugboats," in *Robotics and Automation, 2008. ICRA 2008. IEEE International Conference on*, May 2008, pp. 1489–1494.
- [6] J. Esposito, M. Feemster, and E. Smith, "Cooperative manipulation on the water using a swarm of autonomous tugboats," in *Robotics and Automation, 2008. ICRA 2008. IEEE International Conference on*, May 2008, pp. 1501–1506.
- [7] V. Braitenberg, *Vehicles: Experiments in Synthetic Psychology*. Cambridge, MA: MIT Press, 1984.
- [8] G. A. S. Pereira, V. Kumar, and M. F. M. Campos, "Decentralized algorithms for multirobot manipulation via caging," *International Journal of Robotics Research*, vol. 23, pp. 783–795, 2002.
- [9] L. E. Dubins, "On curves of minimal length with a constraint on average curvature, and with prescribed initial and terminal positions and tangents," *American Journal of Mathematics*, vol. 79, no. 3, pp. 497–516, 1957.
- [10] X.-N. Bui, J.-D. Boissonnat, P. Soueres, and J.-P. Laumond, "Shortest path synthesis for dubins non-holonomic robot," in *Proc. 1994 Int. Conf. on Robotics & Automation*, May 1994, pp. 2–7.